Dynamics of dendrimer-based polymer networks

A. A. Gurtovenko
Institute of Macromolecular Compounds, Russian Academy of Sciences, Bolshoi Prospect 31, V.O., St. Petersburg, 199004 Russia; Laboratory of Physics and Helsinki Institute of Physics, Helsinki University of Technology, P.O. Box 1100, FIN-02015 HUT, Finland; and Theoretische Polymerphysik, Universität Freiburg, Hermann-Herder-Str. 3, D-79104 Freiburg, Germany

D. A. Markelov
Faculty of Physics, St. Petersburg State University, Ulyanovskaya Str. 1, Petrodvorets, St. Petersburg, 198504 Russia

Yu. Ya. Gotlib
Institute of Macromolecular Compounds, Russian Academy of Sciences, Bolshoi Prospect 31, V.O., St. Petersburg, 199004 Russia

A. Blumen[a)]
Theoretische Polymerphysik, Universität Freiburg, Hermann-Herder-Str. 3, D-79104 Freiburg, Germany

(Received 5 June 2003; accepted 15 July 2003)

We present a theoretical study of polymer networks, formed by connecting dendritic building blocks (DBB's). We concentrate on the Rouse dynamics of such networks and perform our study in two steps, considering first single generalized dendrimers (GD's) and then networks formed by such DBB's. In GD's the functionality f of the inner branching points may differ from the functionality f_c of the core. The GD's cover wide classes of macromolecules, such as the ''classical'' dendrimers ($f_c=f$), the dendritic wedges ($f_c=f-1$), and the macromolecular stars ($f_c>2$, $f=2$). Here we present a systematic, analytic way which allows us to treat the dynamics of individual GD's. Then, using a general approach based on regular lattices formed by identical cells (meshes) we study the dynamics of GD-based polymer networks. Using analytical and numerical methods we determine the storage and loss moduli, $G'(\omega)$ and $G''(\omega)$. In this way we find that the intradendrimer relaxation domain of $G'(\omega)$ becomes narrower when M_{cr}, the number of connections between the neighboring DBB's, increases. This effect may be understood due to the exclusion of the longest DBB relaxation times from the spectrum of the network, given that the additional connections hinder the mobility of the peripheral DBB branches. We expect that such effects may be readily observed through appropriate mechanical experiments. © *2003 American Institute of Physics.* [DOI: 10.1063/1.1606675]

I. INTRODUCTION

Dendrimers, being perfectly symmetrical, branched structures have attracted much attention during the past two decades.[1–3] The dendrimers display a series of unique physical and chemical properties which strongly depend on their generation (or, equivalently, on their size). Essentially, the treelike dendrimer topology leads to a very fast increase (which depends exponentially on the generation) of the number of peripheral groups. Therefore, among a plethora of potential applications, dendrimers seem to be ideal candidates for serving as building blocks in the construction of new types of hybrid polymer materials with well-structured, complex architectures. As examples, one can mention here side chain dendritic polymers consisting of linear chains with pendant dendritic groups[4–7] and polymer networks bearing dendritic wedges in the middle of network strands.[8]

In this paper we study theoretically one particular class of polymer networks, namely structures made from dendritic building blocks (DBB's). Recently such networks have attracted much attention.[9–12] The connections between the DBB's can be permanent (one has then permanently cross-linked networks) as well as transient (which leads to physical networks). Such DBB-based polymer networks are of special interest, because they exemplify materials with two levels of structural organization.[13] Here we will study the dynamical properties of permanently cross-linked DBB-based networks, using approaches previously developed by some of us.[14,15]

We focus on the free-draining Rouse description.[16,17] Such an approach is definitely simplified; it does not take into account the excluded volume and the hydrodynamic interactions. Nevertheless, as we have shown in our previous study of side chain dendritic polymers,[18] it allows us to capture the essential features of the viscoelastic mechanical behavior, features which reflect the complex underlying topology.

The paper is organized as follows: Section II describes the theoretical approach used here, which centers on evaluating the storage modulus, $G'(\omega)$, and the loss modulus $G''(\omega)$; these dynamical quantities are readily monitored through viscoelastic experiments. The following three sec-

a)Author to whom correspondence should be addressed. Electronic mail: blumen@physik.uni-freiburg.de

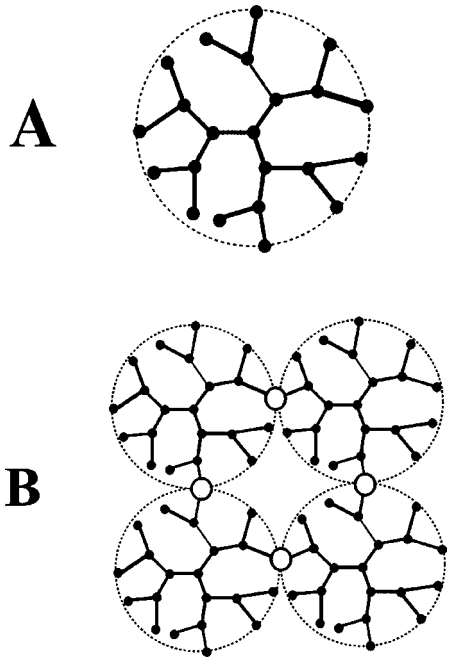

FIG. 1. Examples for the polymer systems under study. Shown are (A) a single dendrimer and (B) the first connecting steps of four such dendrimers in the building of a 2D polymer network.

tions are devoted to the study of the specific systems we are interested in. We proceed in two steps: In Sec. III we consider the Rouse dynamics of single (unconnected) generalized dendrimers (GD's). Here we extend the theoretical approach developed previously for ''classical'' dendrimers[19] and for dendritic wedges[18] to wider classes of dendritic structures, the GD's; in GD's the functionalities of the core and of the inner branching points are independent of each other. In Sec. IV we recall a general method for determining the dynamics of networks consisting of identical cells (meshes) of arbitrary internal structure, cells which are connected into regular (say, cubic or square) lattices. In Sec. V we apply this approach to GD-based polymer networks, and study in particular how the number of connections between neighboring DBB's affects the dynamics of the resulting, global network. In Sec. VI we end the paper with a short summary and conclusions.

II. THEORETICAL MODEL

As stressed, we develop our study of the dynamics of GD-based polymer networks in two steps: First, we focus on single (unconnected) GD's; then we study networks formed from such GD's, see Fig. 1 as an example. We model both the single GD and also the GD-based polymer networks by representing their monomers through beads, attached to each other by elastic springs with elasticity constant K. In this way we treat the dynamics of the systems under study in the framework of the so-called generalized Gaussian structures[20–22] (GGS's). The GGS's represent the extension of the classical Rouse model[16,17] for linear polymer chains to systems of arbitrary topology. For simplicity, we will let all beads of the GGS be subject to the same friction constant ζ with respect to the effective viscous medium (the solvent). Clearly, we aim to have a very simple description; note that the GGS approach allows extensions, such as having beads of different kinds differ in their friction constants.[23]

The Langevin equation of motion for the lth bead of the GGS reads then

$$\zeta \frac{d\mathbf{R}_l(t)}{dt} + K \sum_{m=1}^{N_{\rm tot}} A_{lm} \mathbf{R}_m(t) = \zeta \mathbf{w}_l(t), \tag{1}$$

where $\mathbf{R}_l(t)$ is the position vector of the lth GGS bead, $\mathbf{A} = \{A_{lm}\}$ is the connectivity matrix of the given GGS (here: GD and GD-based networks), and $N_{\rm tot}$ is the total number of beads (monomers) in the GGS considered. In Eq. (1) the nondiagonal element A_{lm} equals (-1) if the lth and mth beads are connected, and 0 otherwise; the diagonal element A_{mm} equals the number of bonds emanating from the mth bead. The thermal noise $\zeta \mathbf{w}_l(t)$ is assumed to be Gaussian, with $\langle \mathbf{w}_l(t) \rangle = 0$ and $\langle \mathbf{w}_{l\alpha}(t) \mathbf{w}_{m\beta}(t') \rangle = 2k_B T \delta_{lm} \delta_{\alpha\beta} \times \delta(t-t')/\zeta$ (here α and β denote the x, y, and z directions).

Now, a typical macroscopic way to test the response of polymeric media consists in measuring the complex (shear) modulus $G^*(\omega)$, which sets in under the influence of an external harmonic strain field;[24] this field acts on the polymer through the solvent and produces stress. The theoretical determination of $G^*(\omega)$ proceeds along classical lines for Rouse-type models, see, e.g., Refs. 17 and 25. In this way, for single GGS's (this corresponds to very dilute solutions) the storage modulus $G'(\omega)$ and the loss modulus $G''(\omega)$ [these are the real and the imaginary parts of $G^*(\omega)$] are given by[17]

$$G'(\omega) = C \frac{1}{N_{\rm tot}} \sum_{i=2}^{N_{\rm tot}} \frac{(\omega \tau_0 / 2\lambda_i)^2}{1 + (\omega \tau_0 / 2\lambda_i)^2} \tag{2}$$

and

$$G''(\omega) = C \frac{1}{N_{\rm tot}} \sum_{i=2}^{N_{\rm tot}} \frac{\omega \tau_0 / 2\lambda_i}{1 + (\omega \tau_0 / 2\lambda_i)^2}. \tag{3}$$

In Eqs. (2) and (3) C equals $\nu k_B T$, where ν is the number of beads (monomers belonging to polymers) per unit volume in the system (macromolecules and solvent) under study; the λ_i are the eigenvalues of the connectivity matrix $\mathbf{A}$ of the given GGS, and $\tau_0 = \zeta/K$ is the characteristic relaxation time. We have chosen the unique, vanishing eigenvalue of the GGS to be λ_1, i.e., we set $\lambda_1 = 0$. Now λ_1 corresponds to the translation of the system as a whole, and it does not contribute to the moduli; hence the sums in Eqs. (2) and (3) start with $i = 2$. Note also the factor 2 in the relaxation times $\tau_i = \tau_0 / 2\lambda_i$ of Eqs. (2) and (3); this factor arises from the second moment of the displacements involved in computing the stress, and we refer to Ref. 17 for a detailed derivation of this fact.

It is noteworthy that even for concentrated solutions, as long as entanglement effects are still negligible (this holds for polymers of low molecular weight), $G'(\omega)$ and $G''(\omega)$ continue to follow the structure of Eqs. (2) and (3), the only difference[24] being a change in the prefactor C. Given that we are mostly interested in the slopes of $G'(\omega)$ and $G''(\omega)$, we will present in the following all our results in terms of the reduced storage and loss moduli, $[G'(\omega)]$ and $[G''(\omega)]$;

these are obtained by setting $C=1$ in Eqs. (2) and (3). Note also the fundamental fact that the eigenfunctions of the connectivity matrix of the GGS do not appear in Eqs. (2) and (3); in the Rouse GGS scheme the shear modulus $G^*(\omega)$ depends only on the eigenvalues. Thus, in order to be able to evaluate $G'(\omega)$ and $G''(\omega)$, it suffices to determine the eigenvalues λ_i (or the relaxation times τ_i) only. This simplifies considerably the solution of the dynamical problem for the GD systems we are interested in.

III. SINGLE GENERALIZED DENDRIMERS

We begin by considering the Rouse dynamics of single GD's. Now the dendrimer problem has encountered much theoretical interest, both in what analytical works on the equilibrium and dynamic properties are concerned,[26–38] as well as in terms of efforts based on computer simulations.[39–43] Most of the existing analytical studies on the dynamics of polymers use the Rouse or the Zimm description and require at a certain stage the diagonalization of the corresponding connectivity matrices by means of analytical[26,28,31] or numerical methods.[32–34,37,38] Now, for very large structures [large N_{tot} in Eq. (1)] numerical diagonalization methods are extremely time consuming; given that all the eigenvalues are needed, today's reasonable limit (in terms of computer time and accuracy) is around $N_{\mathrm{tot}}\simeq 10^4$. Also, depending on the structure, the direct analytical diagonalization of the connectivity matrices is in general (if at all possible) very cumbersome. Recently, we proposed to use for dendrimer-type structures an approach which allows us to find the eigenvalues (and the corresponding relaxation times) in a more analytically minded way.[18,19] The method was first developed for ''classical'' dendrimers[19] (the functionality of a core is the same as that of the inner beads), and then applied to dendritic wedges[18] (a wedge has one main branch less than the classical dendrimer).

However, more general structures are possible, e.g., in which the functionality of the inner branching points and the functionality of the core differ.[35,36] In this paper we extend our analytical approach to finding the eigenvalues to these more general cases. Now, a generalized dendrimer, GD, is characterized by the functionality of the core, f_c, by the functionality of the other inner branching points, f, and by the number of generations, g. Such GD's represent a whole series of structures, which include the classical dendrimers[19] ($f_c=f$) and the dendritic wedges[18] ($f_c=f-1$) previously considered. Furthermore, also star polymers are GD's; for star polymers $f=2$ and f_c is the number of arms.

Exemplarily, we depict in Fig. 2 a GD with $f_c=4$ and $f=3$. Given that the generation zero, $g=0$, consists of the core (the central bead) of the GD, Fig. 2 shows the GD at generation $g=3$. Now, a GD with given f_c, f, and g consists of N_d monomers (beads), where

$$N_d=f_c\frac{(f-1)^g-1}{f-2}+1 \quad \text{for } f\geqslant 3 \tag{4}$$

and

$$N_d=(f_c g+1) \quad \text{for } f=2. \tag{5}$$

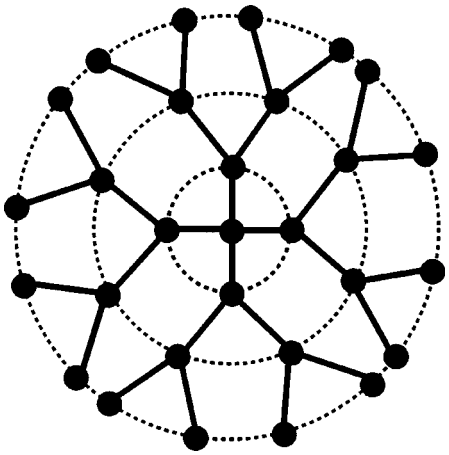

FIG. 2. A generalized dendrimer (GD) of third generation ($g=3$) which has f_c, the core functionality equal to 4, and f, the functionality of the inner branching points equal to 3.

In order to find analytically the eigenvalues of such a GD, it is important, as in our former studies,[18,19] to focus on the underlying topological symmetry; in fact, taking this symmetry already at a very early stage into account, simplifies considerably the analytical procedure. Fundamental here is to note that the eigenmodes of the GD belong to two general classes: Class (i) involves normal modes in which the central core is mobile, class (ii) consists of normal modes with an immobile central core.

A method which allows to determine analytically the eigenvalues and eigenfunctions of GD's is presented in the Appendix; the procedure is similar to our work in Refs. 18 and 19. Summarizing the results of the Appendix, normal modes with a mobile core, class (i), have eigenvalues λ_k of the form

$$\lambda_k=f-2\sqrt{f-1}\cos\psi_k, \tag{6}$$

see Eq. (A8), the ψ_k obeying Eq. (A11):

$$\sin(g+1)\psi_k=\frac{f-f_c-1}{\sqrt{f-1}}\sin g\psi_k. \tag{7}$$

When the inequality of Eq. (A12), $(g+1)/g>|f-f_c-1|/\sqrt{f-1}$, holds, Eq. (6) leads to a total of g distinct solutions. Otherwise, i.e., for $(g+1)/g\leqslant|f-f_c-1|/\sqrt{f-1}$, one has only $(g-1)$ ''spatially periodic'' normal modes, see Eqs. (6) and (7). In this case there appears one additional spatially exponential normal mode. There are now two cases to consider for the spatially exponential normal mode. When $(f-f_c-1)$ is positive, the new eigenvalue reads

$$\Lambda=f-2\sqrt{f-1}\cosh\psi, \tag{8}$$

in which ψ fulfills

$$\sinh(g+1)\psi=\frac{f-f_c-1}{\sqrt{f-1}}\sinh g\psi; \tag{9}$$

see Eqs. (A14) and (A15). In the opposite case, when $(f-f_c-1)$ is negative, one has another kind of spatially exponential normal mode, whose eigenvalue is given by

$$\Lambda = f + 2\sqrt{f-1}\cosh\psi, \tag{10}$$

where ψ is determined from

$$\sinh(g+1)\psi = -\frac{f-f_c-1}{\sqrt{f-1}}\sinh g\psi; \tag{11}$$

see Eqs. (A17) and (A18). Moreover, the case $f-f_c-1=0$ need not be considered here, since for it $(g+1)/g>0$ always holds; it corresponds to dendritic wedges, whose class (i) modes are all spatially periodic.

We end the considerations to class (i) by noting that the eigenvalue $\lambda_1=0$ also belongs to it; λ_1 corresponds to the displacement of the dendrimer as a whole, under the influence of fluctuating forces. Note that the $(g+1)$ eigenvalues found for the normal modes of class (i) are nondegenerate; the situation is in general distinct for the modes of class (ii), as we will show in the following.

Before doing this, we first stop to remark that GD's have in general in class (i) *both* spatially periodical and spatially exponential normal modes. This differs from the situation for classical dendrimers[19] and for dendritic wedges,[18] where for class (i) only spatially periodic normal modes exist. It is namely straightforward to verify that for dendrimers, $f_c=f$, and for dendritic wedges, $f_c=(f-1)$, the inequality of Eq. (A12) is automatically fulfilled. For GD's it is important to notice that in class (i) the eigenvalue connected to a spatially exponential normal mode (when it exists) does not decrease strongly with increasing g, see the Appendix; in class (i) the minimal, nonvanishing eigenvalue is almost independent of N_d (or, for that matter, of g). Hence, as found earlier for the classical dendrimers,[19,31] the normal modes which determine the long time behavior belong to class (ii).

The normal modes of class (ii) have an immobile core. We remark that for this class the eigenvalues and the structure of the eigenfunctions are the same as for the classical dendrimers[19] and for the dendritic wedges.[18] For f and g fixed, changes in f_c $(f_c\geqslant 2)$ lead only to changes in the degeneracy of the eigenvalues. In the special case when only the core is immobile, the eigenvalues λ_k are again given by Eq. (6) but the ψ_k fulfill now

$$\sin(g+1)\psi_k = \sqrt{f-1}\sin g\psi_k; \tag{12}$$

see Eq. (A25). Again we have a situation in which the number of distinct solutions ψ_k depends on a relation between the parameters of the system under study. Thus Eq. (12) provides a total of g distinct solutions if $(g+1)>\sqrt{f-1}g$. Note that this condition is fulfilled only in three cases, namely for $(f=3;g=1)$, for $(f=3;g=2)$, and for $(f=4;g=1)$. In all other cases, i.e., for $(g+1)\leqslant\sqrt{f-1}g$, Eqs. (6) and (12) give only $(g-1)$ solutions. Then, an additional solution appears, leading to an eigenvalue of the form of Eq. (8), with ψ being given by Eq. (A27):

$$\sinh(g+1)\psi = \sqrt{f-1}\sinh g\psi. \tag{13}$$

In contrast to the class (i) normal modes, this eigenvalue is (f_c-1) times degenerate.

In general, the GD motion may be such as to leave large groups of noncore beads immobile; then the eigenvalues λ_k are still given by Eq. (6), with ψ_k obeying Eq. (A30):

$$\sin(g+1-n)\psi_k = \sqrt{f-1}\sin(g-n)\psi_k. \tag{14}$$

Here $0<n<(g-1)$, and n denotes the last generation in which *all* beads are immobile. As in the case of an immobile core, Eq. (14) has $(g-n)$ distinct solutions if $(g-n+1)>\sqrt{f-1}(g-n)$. Otherwise, when $(g-n+1)\leqslant\sqrt{f-1}(g-n)$, Eq. (14) has only $(g-n-1)$ solutions. Then one additional solution appears; it has the form of Eq. (8), where now ψ is

$$\sinh(g-n+1)\psi = \sqrt{f-1}\sinh(g-n)\psi; \tag{15}$$

see Eq. (A32). Common to all these eigenvalues is their degeneracy, which equals $f_c(f-1)^{(n-1)}(f-2)$, where $0<n<(g-1)$. Finally, for $n=(g-1)$ one has the $f_c(f-1)^{(g-2)}(f-2)$-fold degenerate eigenvalue $\lambda=1$; it corresponds to normal modes which involve only peripheral beads.

To conclude this part, it is instructive to stress that the existence of normal modes of two kinds, of spatially periodic kind and of spatially exponential kind, can be readily visualized; spatially periodic normal modes are internal modes inside the GD's sub-branches. For nontrivial GD's $(f>2)$, their eigenvalues are bound from below by $(f-2\sqrt{f-1})$, see Eq. (6), a value independent of g. In contrast, spatially exponential normal modes correspond to the motion of whole sub-branches against each other and may have very small, nonvanishing eigenvalues; such eigenvalues dominate the dynamics at long times. As discussed in the Appendix, the minimal, nonvanishing eigenvalue of the GD, $\lambda_{\min}$, corresponds to a class (ii) normal mode; for large g one has approximately

$$\lambda_{\min}\simeq\frac{(f-2)^2}{(f-1)^{(g+1)}}, \tag{16}$$

see Eq. (A37). In this respect the situation is identical to that found for dendritic wedges[18] and classical dendrimers,[19] given that for all GD's with fixed f and g the class (ii) normal modes are the same, see Appendix.

These findings allow us to study the dynamic properties of GD's in the GGS-framework of Sec. II, given that [based on Eqs. (6)–(15)] we can readily compute *all* the GD eigenvalues (relaxation times) for arbitrary f_c, f, and g. That we indeed obtain in this way *all* the eigenvalues is also shown in the Appendix.

As an illustration, we plot in Fig. 3 the storage, $[G'(\omega)]$, and the loss, $[G''(\omega)]$, moduli of GD's with $f=3$, $g=4$, and varying f_c; in Fig. 3 f_c ranges from 1 to 10. Remarkable for all curves is that they do not show scaling (i.e., a linear dependence in the double logarithmic plot of Fig. 3) in the intermediate frequency domain. In this region $G'(\omega)$ and $G''(\omega)$ reveal the underlying topological structure. Going from $f_c=1$ to $f_c=10$ influences mainly the low-frequency form of the curves, given that the contribution of the maximal relaxation time of the GD (because of the degeneracy) increases with f_c.

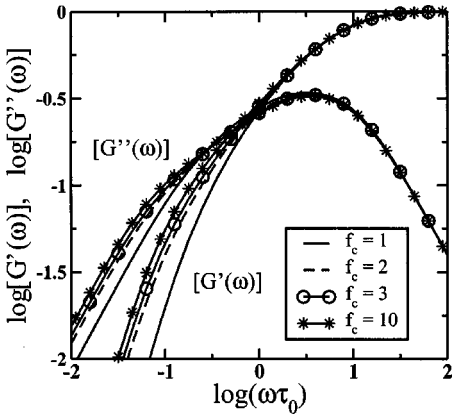

FIG. 3. Reduced storage modulus $[G'(\omega)]$ and loss modulus $[G''(\omega)]$ plotted in double logarithmic scales vs the reduced frequency $\omega\tau_0$. Shown are results for GD's with $f=3$ and $g=4$. The functionality of the core, f_c, takes the values 1, 2, 3, and 10.

IV. NETWORKS BUILT FROM SUBSTRUCTURES (CELLS): THE MODEL

Now we turn to a formalism which allows us to study the dynamics of networks built from topologically complex substructures. In the next section we will apply this method to regular lattices built from GD's. We start by remarking that the study of cross-linked polymer chains which then form regular lattices has a long history;[44–48] treating cross-linked dendritic structures is, however, of quite recent interest.[8,18] Before considering particular networks based on GD's, in this section we recall a general approach developed by some of us[14,15] to treat the dynamics of lattices formed by identical cells (substructures). In former works[14,15] these cells consisted themselves of subunits; here we let the cells have an arbitrary architecture, and require only that they are topologically identical to each other.

We start our presentation based on a (topologically) three-dimensional cubic lattice; the reduction to lower dimensions and the extension to higher topological dimensions are quite straightforward. The elementary cubic cell of the lattice is denoted by a three-component index $\mathbf{\Omega}=(\alpha,\beta,\gamma)$ where α, β, and γ range from 1 to N. We assume that such a cell contains s beads, which we number by the index $j\in\{1,\cdots,s\}$. The whole network consists then of sN^3 beads, numbered by $(j,\mathbf{\Omega})\equiv(j,\alpha,\beta,\gamma)$. As before, all the beads are connected to their neighbors by means of elastic springs which have the same elasticity constant K.

In this case the determination of the eigenvalues of the connectivity matrix $\mathbf{A}$ simplifies considerably, since the elastic term in Eq. (1) reads:[14,15]

$$\sum_{m=1}^{N_{\rm tot}} A_{lm}\mathbf{R}_m(t)=\sum_{i=1}^{s}\sum_{\mathbf{\Omega}'} A_{j\mathbf{\Omega}i\mathbf{\Omega}'}\mathbf{R}_{i\mathbf{\Omega}'}(t)$$
$$=\sum_{i=1}^{s} A_{j\mathbf{\Omega}i\mathbf{\Omega}}\mathbf{R}_{i\mathbf{\Omega}}(t)$$
$$+\sum_{i=1}^{s}\sum_{\substack{\mathbf{\Omega}'\\ \mathbf{\Omega}'\neq\mathbf{\Omega}}} A_{j\mathbf{\Omega}i\mathbf{\Omega}'}\mathbf{R}_{i\mathbf{\Omega}'}(t) \qquad (17)$$

where one lets $l\to(j,\mathbf{\Omega})$ and $m\to(i,\mathbf{\Omega}')$. Due to obvious symmetries, one now sets in Eq. (17) $B_{ji}^{(\rm int)}\equiv A_{j\mathbf{\Omega}i\mathbf{\Omega}}$ and $B_{ji}^{(\rm ext)}(\mathbf{\Delta})\equiv B_{ji}^{(\rm ext)}(\mathbf{\Omega}-\mathbf{\Omega}')\equiv A_{j\mathbf{\Omega}i\mathbf{\Omega}'}$. This leads to[15]

$$\sum_{m=1}^{N_{\rm tot}} A_{lm}\mathbf{R}_m(t)=\sum_{i=1}^{s} B_{ji}^{(\rm int)}\mathbf{R}_{i\mathbf{\Omega}}(t)$$
$$+\sum_{i=1}^{s}\sum_{\mathbf{\Delta}} B_{ji}^{(\rm ext)}(\mathbf{\Delta})\mathbf{R}_{i\mathbf{\Omega}-\mathbf{\Delta}}(t), \qquad (18)$$

where $\mathbf{\Delta}=\mathbf{\Omega}-\mathbf{\Omega}'$ is the relative distance between the lattice cells $\mathbf{\Omega}$ and $\mathbf{\Omega}'$, measured in units of number of cells. In Eq. (18) the matrix $\mathbf{B}^{(\rm int)}=\{B_{ji}^{(\rm int)}\}$ is the connectivity matrix inside a given cell consisting of s beads. On the other hand, the matrices $\mathbf{B}^{(\rm ext)}(\mathbf{\Delta})=\{B_{ji}^{(\rm ext)}(\mathbf{\Delta})\}$ describe the intercell connections: In them the nonzero elements $B_{ji}^{(\rm ext)}(\mathbf{\Delta})$ equal -1; they indicate that bead j of cell $\mathbf{\Omega}$ and bead i of cell $\mathbf{\Omega}'=\mathbf{\Omega}-\mathbf{\Delta}$ are connected by a bond. If one connects the cells in the spirit of Fig. 1, each elementary cell is directly connected to its nearest-neighbor cells only; for a topologically cubic lattice the $\mathbf{\Delta}$ are then restricted to the set $\{(1,0,0),(-1,0,0),(0,1,0),(0,-1,0),(0,0,1),(0,0,-1)\}$ only.

As discussed in Refs. 14 and 15, the procedure is close in spirit to that encountered in the study of crystals;[49–51] the mathematical structure of the theory is identical, but the physical situation is not. In particular, the polymer network is in no way assumed to be translationally invariant.[14,15] Formally now, the ansatz

$$\mathbf{R}_{j\mathbf{\Omega}}(t)\equiv\mathbf{R}_{j\alpha\beta\gamma}(t)=\sum_{k_1,k_2,k_3}\mathbf{C}_{j\mathbf{k}}\exp(i[k_1\alpha+k_2\beta+k_3\gamma])$$
$$\times\exp[-\lambda(\mathbf{k})t/\tau_0], \qquad (19)$$

solves the problem. Here i denotes the imaginary unit, $\tau_0=\zeta/K$ is the characteristic relaxation time, the $\mathbf{C}_{j\mathbf{k}}$ are constants, and the $\mathbf{k}=(k_1,k_2,k_3)$ obey $k_i=2\pi m_i/N$, where the m_i are integers with $0\leqslant m_i\leqslant(N-1)$ for $i=1$, 2, and 3. Again, one should stress that in Eq. (19) the index $\mathbf{k}$ simply counts the eigenvalues (modes), and is not related to a reciprocal wave vector. Setting

$$B_{jl}(\mathbf{k})=B_{jl}^{(\rm int)}+\sum_{\mathbf{\Delta}} B_{jl}^{(\rm ext)}(\mathbf{\Delta})\exp(-i\mathbf{k}\cdot\mathbf{\Delta}) \qquad (20)$$

the Langevin equation of motion, Eq. (1), reads now[14,15]

$$\lambda(\mathbf{k})\mathbf{C}_{j\mathbf{k}}=\sum_{l=1}^{s} B_{jl}(\mathbf{k})\mathbf{C}_{l\mathbf{k}}. \qquad (21)$$

The matrices $\mathbf{B}(\mathbf{k})=\{B_{jl}(\mathbf{k})\}$ carry all the information about the connectivity (inter- and intracell). Since there are N^3 $\mathbf{k}$ values, there are N^3 different $\mathbf{B}(\mathbf{k})$ matrices. The symmetry helped to simplify the problem: instead of having to diagonalize $\mathbf{A}$, which is a $(sN^3\times sN^3)$ matrix, one has now to diagonalize N^3 different $(s\times s)$ matrices.[15]

V. DENDRIMER-BASED LATTICES

Now we apply the general approach of the previous section to our system of interest, and treat topologically regular lattices built from GD's, see for instance Fig. 1(B). We hence assume that the dendritic building blocks (DBB's) are con-

nected with each other in a regular way: We denote by M_{cr} the number of connections stemming from each DBB, divided by the number of its neighboring DBB's. As an example, in Fig. 1(B), given the two-dimensional pattern of the lattice, one has $M_{cr}=4/4=1$.

The case $M_{cr}=1$ corresponds to a slightly connected GD-based network. Values of M_{cr} larger than unity are readily attained. For this we center on the peripheral beads, since they are most prone to serve as connections, given that their functionality inside the GD is less than f. A GD with given f_c, f, and g has $N_{\rm per}$ peripheral beads, where

$$N_{\rm per}=f_c(f-1)^{(g-1)}. \tag{22}$$

In a simple hypercubic geometry each lattice site has $2d_{\rm lat}$ nearest neighbors, where $d_{\rm lat}$ is the dimensionality of the lattice. Setting n for the largest integer not exceeding $(N_{\rm per}/2d_{\rm lat})$, one can then use, in a symmetric way, up to n beads to connect a DBB to one of its neighbors.

In order to apply our general approach we have to specify the matrices $\mathbf{B}^{(\rm int)}=(B_{jl}^{(\rm int)})$ and $\mathbf{B}^{(\rm ext)}(\mathbf{\Delta})=(B_{jl}^{(\rm ext)}(\mathbf{\Delta}))$, see Eq. (20), to the problem at hand. Focussing on Fig. 1(B), a link is established between two GD's by the elimination of one bead, say, through a disproportionation reaction. Evidently, other cross-linking procedures are possible, e.g., through the creation of new bonds. Since we treated such situations in previous work, we prefer to consider here the case of Fig. 1(B). We also stay in the framework of a homopolymer model (all beads in the whole network system have the same friction constants), although the copolymer case may be also considered.[23] Hence, due to the newly created M_{cr} connections between each pair of neighboring cells, each such cell has $M_{cr}d_{\rm lat}$ beads less than the precursor GD with N_d beads, Eq. (4). Such a DBB cell contains thus $s=N_d-M_{cr}d_{\rm lat}$ beads, and the matrix $\mathbf{B}^{(\rm int)}$ can be obtained from that of the original GD by the removal of these $M_{cr}d_{\rm lat}$ beads. Moreover, given that there are $2d_{\rm lat}$ nearest neighbors to each DBB cell, there are $2d_{\rm lat}$ nonvanishing $\mathbf{B}^{(\rm ext)}(\mathbf{\Delta})$; each of these matrices contains M_{cr} nonzero elements equal to (-1); see the previous sections for details.

Now we are ready to perform numerical calculations on networks consisting of DBB's; for this we follow our general scheme discussed in Sec. IV. An interesting question on which we will focus is in how far M_{cr}, the number of connections between pairs of neighboring DBB's, affects the dynamics of the network.

We start at first with DBB's connected into a two-dimensional (2D) square lattice. Here it is worthwhile to recall that such a network is two dimensional only in a topological sense; dynamically, the network moves in the 3D Cartesian space like a fishing net in water. An obvious question is then in how far our results are influenced by the choice of the lattice; we will make some comparisons with 3D lattices at the end of this section.

We start with a fully symmetrical situation so that the symmetry of the DBB matches that of a 2D lattice. Such a situation is, for instance, obtained when f_c, the functionality of the core of the underlying GD, is taken to be $2d_{\rm lat}$, here thus $f_c=4$. In Fig. 4 we plot the reduced storage modulus

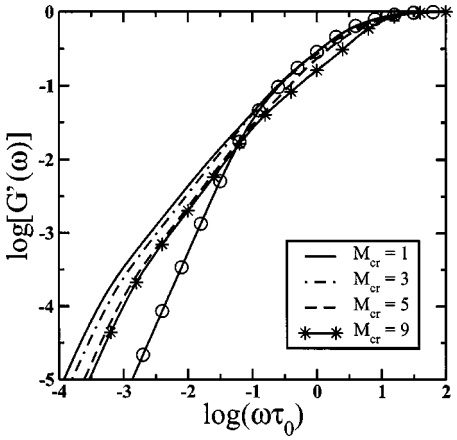

FIG. 4. Reduced storage modulus $[G'(\omega)]$ plotted in double logarithmic scales vs the reduced frequency $\omega\tau_0$. Shown are results for a square (20 $\times$20) lattice based on a GD with $f_c=4$, $f=4$, and $g=3$. The number of connections between the DBB's ranges from $M_{cr}=1$ to $M_{cr}=9$; the latter value leads to a network without dangling bonds. The line with open circles gives the behavior of the single, underlying GD.

$[G'(\omega)]$ for GD's with $f_c=4$, $f=4$, and $g=3$, which are connected into a (20$\times$20) square lattice. We let M_{cr}, the number of connections between neighboring DBB's, vary such that M_{cr} equals 1, 3, 5, and 9. Furthermore, we take care that the connections obey the symmetry requirement; they are then regularly distributed with respect to the underlying GD. Note that in our case here $M_{cr}=9$ corresponds to the situation in which *all* peripheral beads of the underlying GD participate in connections, so that there are no dangling bonds at all. Distinct from it is the case $M_{cr}=1$, in which the network is only slightly connected. Also presented in Fig. 4 is $[G'(\omega)]$ for the underlying GD. Starting with the isolated GD, one has a plateau at very high frequencies and a terminal, ω^2-type behavior at very low frequencies. The frequency region in between is typical for dendrimers: in the doubly logarithmic scales of Fig. 4 the curve has a logarithmic-type behavior.[37,38] Going now to the lattice case, we start with $M_{cr}=1$. The curve at rather high frequencies reveals then the isolated GD behavior of $[G'(\omega)]$. This is followed by a region with a power-law decay, $[G'(\omega)]\sim\omega$, typical for 2D lattices.[46,52,53] Finally, as it is typical for GGS's of finite size, one again reaches at very low frequencies the terminal, ω^2-decay pattern of $[G'(\omega)]$. In Fig. 4 this terminal domain is located at $\log(\omega\tau_0)<-3$.

Increasing M_{cr} leads to a systematic narrowing of the high-frequency region, in which the GD behavior is evident; the curves for larger M_{cr} depart earlier from the curve of the single GD. As we will see in the following, this effect has a generic character, i.e., it does not depend significantly on the DBB parameters f_c, f, and g, nor on the particular type of regular lattice into which the DBB's are connected. This can be explained as follows: The long relaxation times of the single GD are controlled by large amplitude motions. The connections hinder these motions, and force instead the individual DBB to follow the dynamics dictated by the lattice.

In Fig. 5 we plot the reduced storage modulus $[G'(\omega)]$ again for a 2D (20$\times$20) lattice, but built from a larger GD, with $f_c=4$, $f=4$, and $g=4$. The displayed data show the

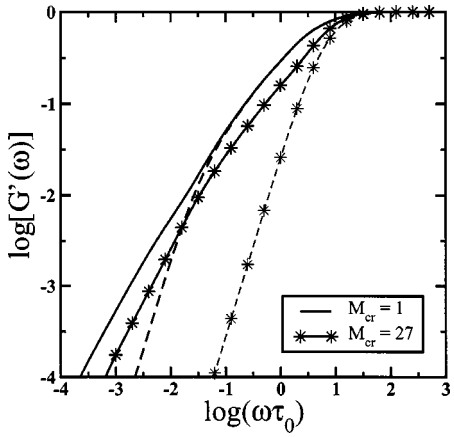

FIG. 5. The same as in Fig. 4 but for DBB's based on a GD with $f_c=4$, $f=4$, and $g=4$. Shown are the results for the two extreme cases: $M_{cr}=1$ and $M_{cr}=27$. Also shown is $[G'(\omega)]$ for the isolated GD (dashed line) and for the same GD, when its peripheral beads are hold fixed (dashed line with stars).

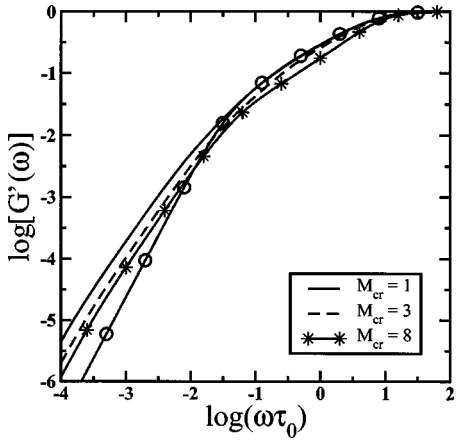

FIG. 7. Reduced storage modulus $[G'(\omega)]$ plotted in double logarithmic scales vs the reduced frequency $\omega\tau_0$. Shown are the results for a cubic ($20\times20\times20$) lattice based on a GD with $f_c=3$, $f=3$, and $g=5$. The number of connections between neighboring DBB's ranges from $M_{cr}=1$ to $M_{cr}=8$. The line with open circles gives $[G'(\omega)]$ for the isolated GD.

extreme cases, namely $M_{cr}=1$ and $M_{cr}=27$; in the latter there are no dangling bonds anymore (note that the terminal, ω^2-type decay of $[G'(\omega)]$ does not yet show up in Fig. 5). Moreover, in Fig. 5 we also display the relaxation behavior of the isolated GD, and also a situation in which all peripheral beads of the GD are hold immobile. From Fig. 5 the narrowing with increasing M_{cr} of the domain of GD relaxation is evident; the narrowing gets even more pronounced when the DBB size increases. Furthermore, we note the appearance with large M_{cr} of a domain intermediate between GD-like and lattice dominated. Also clear from Fig. 5 is that for high M_{cr} the high-frequency domain cannot be represented in terms of a single DBB with all its peripheral beads fixed. This is due to the extremely narrow relaxation spectrum of a DBB with fixed ends, its longest relaxation time being almost independent of its size.[26,28]

As for the loss modulus $[G''(\omega)]$, it turns out to be less sensitive to M_{cr} than $[G'(\omega)]$; see Fig. 6. Here, as usual, $[G''(\omega)]$ displays a maximum, whose position is mostly determined by the high-frequency modes, which in general involve the motion of just a few beads. The dependence of the dynamics on M_{cr} appears predominantly on length scales comparable to the size of the GD. We conclude that the loss modulus $[G''(\omega)]$ is less adequate than $[G'(\omega)]$ to display connectivity-related effects. From Fig. 6 we note as special case the totally connected situation, $M_{cr}=27$. The corresponding curve has its maximum shifted to higher frequencies, when compared to the situation for smaller M_{cr}.

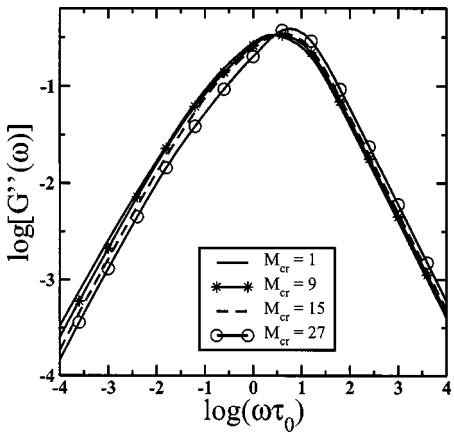

FIG. 6. Reduced loss modulus $[G''(\omega)]$ plotted in double logarithmic scales vs the reduced frequency $\omega\tau_0$. Shown are the results for a square (20×20) lattice based on a GD with $f_c=4$, $f=4$, and $g=4$. Here M_{cr} ranges from $M_{cr}=1$ to $M_{cr}=27$, see text for details.

All the above conclusions have been drawn on the basis of 2D lattices built from DBB's, whose symmetry is consistent with the symmetry of the lattice (in particular, we chose $f_c=4$). To gain an idea on how this point affects our results, we calculated the dynamic moduli for the same 2D lattice built from DBB's which are not symmetrical with respect to the lattice, namely for $f_c=3$ (the data are not shown). We found that all our main conclusions are unaffected by the choice of f_c.

Now we turn to a 3D cubic lattice, obtained by connecting DBB's. Such a structure continues to be rather simple; possibly, however, it may represent real networks closer.[54] In Fig. 7 we present our numerical results for the storage modulus $[G'(\omega)]$ of a 3D ($20\times20\times20$) lattice, built from trifunctional dendrimers of generation 5 ($f_c=3$, $f=3$, and $g=5$). With increasing M_{cr} we observe the same trend as before: going from $M_{cr}=1$ to $M_{cr}=8$ leads to a stronger departure of the $[G'(\omega)]$ from the curve corresponding to the isolated GD; the boundary of the region in which these curves differ shifts to higher frequencies.

We conclude by noting that the main significant difference between 2D and 3D GD-based model networks is to be found in the relaxation domain determined by the lattice. To demonstrate this, we plot in Fig. 8 for $M_{cr}=1$ the storage modulus $[G'(\omega)]$ for DBB's connected into a 2D and into a 3D network. Here the DBB's are based on trifunctional dendrimers ($f_c=3$, $f=3$, and $g=5$). The difference in $[G'(\omega)]$ can now be seen in the domain of frequencies where the relaxation starts to differ from that of the single GD, on the low-frequency side. Here one expects a behavior close to

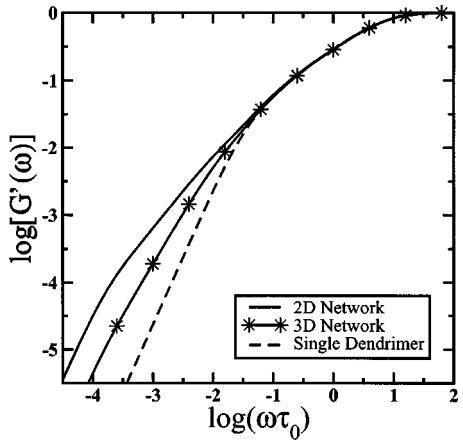

FIG. 8. Reduced storage modulus $[G'(\omega)]$ plotted in double logarithmic scales vs the reduced frequency $\omega\tau_0$. Shown are results for a square (20 $\times$20) lattice and for a cubic (20$\times$20$\times$20) lattice based on a GD with $f_c=3$, $f=3$, and $g=5$. Here $M_{cr}=1$. The dashed line gives $[G'(\omega)]$ for the isolated GD.

$[G'(\omega)]\sim\omega^{3/2}$ for three-dimensional[47,48] and $[G'(\omega)]\sim\omega$ for two-dimensional[46,52,53] networks, a fact which is fulfilled in Fig. 8. At even lower frequencies the behavior crosses over to the universal, $[G'(\omega)]\sim\omega^2$ scaling law. Now, both 2D and 3D regular lattices are very idealized models for general DBB networks; nonetheless, the finding that connecting DBB's into a network (by which the mobility of their peripheral monomers is hindered) leads to the narrowing of the internal relaxation domain of the DBB is a fact of general validity, which may be used as a signature for cross linking.

VI. CONCLUSIONS

In this paper we presented a theoretical study of the dynamics of dendrimer-based polymer networks. In such structures, the networks are created by connecting DBB's. Our goal was to determine the influence of M_{cr}, the number of connections between the neighboring DBB's, on the mechanical characteristics (such as the storage and the loss moduli) of the network. We modeled the systems by GGS, a method which extends Rouse's ideas to hyperbranched and to multiply-connected objects. We performed our study in two steps, considering first isolated GD's and then regular networks formed by such GD's.

First, we determined analytically the eigenvalues (relaxation times) and the eigenfunctions for the generalized dendrimers (GD's); GD's are given by f_c, the functionality of the core, *f*, the functionality of the inner branching points, and *g*, the generation. Such GD's describe a wide class of structures, among which are the classical dendrimers ($f_c=f$), the dendritic wedges ($f_c=f-1$), and the macromolecular stars ($f_c>2$, $f=2$). Our general results here are fully consistent with previously undertaken studies.[18,19,31]

Then, we recalled a general method for determining in the GGS framework the dynamics of regular lattices formed by identical cells (domains) of arbitrary internal topology. We applied this method to regular (2D as well as 3D) lattices, obtained by connecting DBB's. Our main variable here was the number of connections, M_{cr}, between neighboring DBB's. Using analytical and numerical methods we evaluated the dynamical shear modulus of the system under study, while highlighting the role played by M_{cr}. The fact that an increase in M_{cr} is linked to a hindrance of the mobility of the peripheral DBB groups leads to the exclusion of the long relaxation times of the DBB's from the relaxation of the whole lattice. With increasing M_{cr} the storage modulus $[G'(\omega)]$ of the network deviates more and more from the behavior of $[G'(\omega)]$ for the isolated GD. This effect is very general; in particular, it is almost independent of the f_c, *f*, and *g* parameters and of the type (2D or 3D) of the underlying lattice. We expect that the effects discussed here will be readily observable through appropriate mechanical experiments on dendrimer-based polymer networks.

ACKNOWLEDGMENTS

Helpful discussions with Dr. Sergey V. Lyulin are gratefully acknowledged. This work was supported by the Fonds der Chemischen Industrie, by the BMFB, by the DFG, and by the INTAS (Grant No. 00-712). A.A.G. acknowledges the support of the Alexander von Humboldt Foundation and of the Academy of Finland (Grant No. 202598). Y.Y.G. acknowledges the support of the Russian Federal Program "Integration," of the Russian Foundation of Basic Research (Grant No. 02-03-33132), and of the ESF Scientific Program SUPERNET.

APPENDIX: EIGENVALUES AND EIGENFUNCTIONS OF A GENERALIZED DENDRIMER

Here we present the determination of the eigenvalues and eigenfunctions of GD's which are characterized by f_c, the functionality of the core, by *f*, the functionality of the other inner beads, and by *g*, the number of generations. Our procedure follows closely that of the Appendix of Ref. 18, so that we focus on the differences encountered in going from the dendritic wedge treated in Ref. 18 to our general case here; note that for the wedge $f_c=(f-1)$ holds.

1. Mobile core

When the core is mobile in general all GD beads may be involved in the motion.[18,19,31] Since each inner GD bead is connected to one bead from the previous and $(f-1)$ beads from the next generation, the Langevin equations of motion for the inner GD beads read [see Eq. (1)]

$$\zeta\frac{d\mathbf{R}_{j,m}(t)}{dt}+K\left[f\mathbf{R}_{j,m}(t)-\mathbf{R}_{j-1,n}(t)-\sum_{l=1}^{f-1}\mathbf{R}_{j+1,l}(t)\right]=0. \tag{A1}$$

Here $\mathbf{R}_{j,m}(t)$ is the position vector of the *m*th bead of generation *j*, where the index *j* for the inner beads lies in the range $0<j<g$ ($j=0$ corresponds to the core) and $\mathbf{R}_{j-1,n}(t)$ and $\mathbf{R}_{j+1,l}(t)$ ($l=1,\ldots,f-1$) correspond to the locations of the nearest neighbors to $\mathbf{R}_{j,m}(t)$. As in Ref. 18 we set the right-hand side of Eq. (A1) to zero, since the averages we are interested in imply only linear relations of the normal modes. The system of Eq. (A1) can be solved by the transformation[18]

$$\mathbf{R}_{j,m}(t)=\sum_k \mathbf{C}_k \Pi_k(j,m)\exp[-\lambda_k t/\tau_0], \tag{A2}$$

where $\tau_0=\zeta/K$ is the characteristic relaxation time of the GD, $\mathbf{C}_k$ are j-independent constants, λ_k are the eigenvalues, and $\Pi_k(j,m)$ are the eigenfunctions corresponding to Eq. (A1). The relaxation times τ_k are uniquely determined by the eigenvalues λ_k through $\tau_k=\tau_0/\lambda_k$. Inserting Eq. (A2) into Eq. (A1) leads to

$$(-\lambda_k)\Pi_k(j,m) + \left[f\Pi_k(j,m)-\Pi_k(j-1,n)-\sum_{l=1}^{f-1}\Pi_k(j+1,l)\right]=0. \tag{A3}$$

As before,[18,19] also for GD's the normal modes can be characterized by motions involving one ''root'' bead and all of its descendants of higher generations. For any subwedges having as ancestor the same root, beads which belong to the same generation move in the same manner.[18,19] For motions in which the core is the root one thus has $\Pi_k(j,m)=\Pi_k(j)$; see also Refs. 19 and 18 and Fig. 3 of Ref. 31. It this way Eq. (A3) gets simplified to

$$(-\lambda_k)\Pi_k(j)+[f\Pi_k(j)-\Pi_k(j-1)-(f-1)\Pi_k(j+1)]=0. \tag{A4}$$

One solution of Eq. (A4) is $\Pi_k(j)=\text{const}$; the corresponding eigenvalue is $\lambda_1=0$. The other solutions are best obtained using the substitution $\Pi_k(j)=(f-1)^{-j/2}\Phi_k(j)$, which leads to[18,19]

$$(f-\lambda_k)\Phi_k(j)-\sqrt{f-1}[\Phi_k(j+1)+\Phi_k(j-1)]=0. \tag{A5}$$

Equation (A5) holds for all inner beads, $0<j<g$. The peripheral beads, $j=g$, obey

$$(1-\lambda_k)\Phi_k(g)-\sqrt{f-1}\Phi_k(g-1)=0 \tag{A6}$$

while for the case $j=0$ one has

$$(f_c-\lambda_k)\Phi_k(0)-\frac{f_c}{\sqrt{f-1}}\Phi_k(1)=0. \tag{A7}$$

Note that only in Eq. (A7) the parameter f_c enters explicitly. Hence this equation is the one that differentiates arbitrary GD's, classical dendrimers[19] (for which $f_c=f$), and dendritic wedges[18] (for which $f_c=f-1$).

Now, a general group of eigenfunctions $\Phi_k(j)$ to the system of Eqs. (A5)–(A7) can be expressed as linear combinations of the functions $\Phi_k^c(j)=\cos j\psi_k$ and $\Phi_k^s(j)=\sin j\psi_k$, where the ψ_k will be determined in the following. It is namely a simple matter to verify that $\Phi_k^c(j)$ and $\Phi_k^s(j)$ satisfy Eq. (A5) for the eigenvalue[18,19]

$$\lambda_k=f-2\sqrt{f-1}\cos\psi_k. \tag{A8}$$

Equations (A6) and (A7) fix now the form of $\Phi_k(j)$. It is easy to check that the linear combination

$$\Phi_k(j)=[\sqrt{f-1}(f_c-f)+[2(f-1)-f_c]\cos\psi_k]\Phi_k^s(j) + [f_c\sin\psi_k]\Phi_k^c(j), \tag{A9}$$

which can be rewritten as

$$\Phi_k(j)=(f-1)\sin(j+1)\psi_k+(f_c-f)\sqrt{f-1}\sin j\psi_k + (f-f_c-1)\sin(j-1)\psi_k, \tag{A10}$$

solves both Eq. (A7) and also Eq. (A6) when the ψ_k obey

$$\sin(g+1)\psi_k=\frac{f-f_c-1}{\sqrt{f-1}}\sin g\psi_k. \tag{A11}$$

We stop to emphasize that by setting $f_c=f$ or $f_c=(f-1)$ in Eqs. (A10) and (A11), we recover the previously obtained results for classical dendrimers[19] and for dendritic wedges,[18] respectively.

Now we turn to the question of the number of distinct eigenvalues obtainable from Eq. (A11). As previously discussed by some of us for dendritic wedges,[18] in class (ii), Eqs. (A8) and (A11) lead to either $(g-1)$ or to g distinct eigenvalues. This depends on whether $(g+1)/g$ is larger or smaller than $|f-f_c-1|/\sqrt{f-1}$. For

$$\frac{(g+1)}{g}>\frac{|f-f_c-1|}{\sqrt{f-1}} \tag{A12}$$

Eqs. (A8) and (A11) lead to a total of g distinct solutions; otherwise the number of distinct solutions is $(g-1)$. We note that Eq. (A12) is automatically fulfilled for the classical dendrimers[19] ($f_c=f$) and for the dendritic wedges[18] ($f_c=f-1$). In other words, all their class (i) nonvanishing eigenvalues and corresponding eigenfunctions are of spatially periodic type.

When Eq. (A12) does not hold there appear, as for class (ii) normal modes,[18] additional eigenfunctions. We note first that the combination

$$\Phi(j)=(f-1)\sinh(j+1)\psi+(f_c-f)\sqrt{f-1}\sinh j\psi + (f-f_c-1)\sinh(j-1)\psi \tag{A13}$$

fulfills Eq. (A5) for the eigenvalue

$$\Lambda=f-2\sqrt{f-1}\cosh\psi. \tag{A14}$$

Inserting Eq. (A13) into Eqs. (A6) and (A7) leads to the following equation for ψ:

$$\sinh(g+1)\psi=\frac{f-f_c-1}{\sqrt{f-1}}\sinh g\psi. \tag{A15}$$

One can easily demonstrate (see Ref. 18) that apart from the trivial solution $\psi=0$, Eq. (A15) has a single additional solution ψ if and only if $(g+1)/g\leqslant|f-f_c-1|/\sqrt{f-1}$ and $(f-f_c-1)>0$.

Interestingly, when $(f-f_c-1)<0$ and $(g+1)/g\leqslant|f-f_c-1|/\sqrt{f-1}$, Eq. (A15) has no nontrivial solutions. It turns out that in this case the spatially exponential eigenmode still exists; now its eigenfunction ''alternates'' from generation to generation, namely it is given by

$$\Phi(j)=(-1)^j[(f-1)\sinh(j+1)\psi-(f_c-f)\sqrt{f-1}\sinh j\psi + (f-f_c-1)\sinh(j-1)\psi]. \quad \text{(A16)}$$

One should note the factor $(-1)^j$ when comparing Eq. (A16) with Eq. (A13). It is now straightforward to verify that this eigenfunction corresponds to the eigenvalue

$$\Lambda=f+2\sqrt{f-1}\cosh\psi, \quad \text{(A17)}$$

where ψ is determined by

$$\sinh(g+1)\psi=-\frac{f-f_c-1}{\sqrt{f-1}}\sinh g\psi. \quad \text{(A18)}$$

Because of the change of sign in this condition, in a similar way as above, it follows that Eq. (A18) has a single, nontrivial solution if and only if $(f-f_c-1)<0$ and $(g+1)/g \leqslant |f-f_c-1|/\sqrt{f-1}$.

We stop to note the differences between Eqs. (A8), (A10), and (A11) on one hand and Eqs. (A13)–(A18) on the other. They lead to a total of g nondegenerate class (i) eigenmodes, which can be categorized into two groups: The first group is given by spatially periodic normal modes, the second group contains at most one spatially exponential normal mode. Including the eigenvalue $\lambda_1=0$ we hence have a total of

$$N_\lambda^{(1)}=g+1 \quad \text{(A19)}$$

distinct, class (i) eigenvalues (i.e., relaxation times).

Before turning to the class (ii) normal modes, it is very instructive at this point to estimate the value of the minimal nonvanishing eigenvalue in class (i). From Eq. (A8) it follows that for spatially periodical normal modes the eigenvalues are bound from below by $f-2\sqrt{f-1}$, which is always positive. Furthermore, these eigenvalues do not depend on g. The Λ eigenvalue of Eq. (A14) for class (i) normal modes can be estimated as follows:[18] Using the new variable $z=\exp\psi$ one can rewrite Eq. (A15) in the form

$$z=\frac{f-f_c-1}{\sqrt{f-1}}\frac{1-z^{-2g}}{1-z^{-2g-2}}. \quad \text{(A20)}$$

In terms of z the eigenvalue Λ, Eq. (A14), reads

$$\Lambda=f-\sqrt{f-1}(z+z^{-1}). \quad \text{(A21)}$$

For large g one can obtain z iteratively from Eq. (A20). Evidently, a starting point $(g\to\infty)$ is $z^{(0)}\simeq(f-f_c-1)/\sqrt{f-1}$ [note that here $(f-f_c-1)$ is positive and that $(f-f_c-1)/\sqrt{f-1}>(g+1)/g>1$] from which, with Eq. (A21), it follows that

$$\Lambda^{(0)}=(f_c+1)-\frac{f-1}{f-f_c-1}. \quad \text{(A22)}$$

We stress that, similar to spatially periodic normal modes, the eigenvalue for the spatially exponential mode is bound from below by $\Lambda^{(0)}$, which does not depend on g. Note that the case $f_c=(f-1)$ [when one has a singularity in Eq. (A22)] is not included, because for $f_c=(f-1)$ no eigenvalue of Λ type exists, see Eq. (A12). Also, care has to be taken for the special case $f_c=(f-2)$, for which one might infer $\Lambda^{(0)}=0$, see Eq. (A22). However, this case, $f_c=(f-2)$, is again not consistent with the appearance of a spatially exponential normal mode, see Eq. (A12), and therefore has to be excluded from consideration. Repeating all the above arguments for the exponential eigenmode of ''alternating'' type, see Eqs. (A17) and (A18), one can again show that $\Lambda^{(0)}$, given by Eq. (A22), is a lower boundary for Λ. Thus for class (i) normal modes the eigenvalue Λ is practically independent of the size of the dendrimer (i.e., of the number of generations g). As we will see in the following, this is not the case for class (ii) normal modes.

2. Immobile core

The next group of motions which we consider imply an immobile core,[18,19,31] i.e., they are class (ii) normal modes. Here, because of the inherent symmetry, one has for GD's with given f and g the same set of eigenvalues (relaxation times) as for the classical dendrimers[19] and the dendritic wedges[18] with the same f and g. The only difference consists in the degeneracy of these eigenvalues. To see this, consider first the case when the normal mode involves a mobile next-neighbor bead to the core. Then the degeneracy of the corresponding eigenvalues will be here (f_c-1)-fold, as compared to $(f-1)$-fold for the classical dendrimer[19] and to $(f-2)$-fold for the dendritic wedge.[18] This can be seen as follows: One can choose as eigenmodes those in which most of the neighboring beads of the core and their descendents are immobile, so only two neighboring beads (and their subwedges) move against each other, while the core stays immobile.[18,19,31] These beads act as ''roots.'' Now focusing on such one root, one can pick for it exactly (f_c-1) different partner roots, by which one obtains a set of corresponding, (f_c-1), linearly independent normal modes. It is then easy to verify that the other normal modes of this class follow by a linear operation (a subtraction) from the members of the set.[18,19,31]

Thus, for class (ii) normal modes, the problem involves separated, mobile subwedges. The problem has been discussed in details in Ref. 18, so that we can report the results, restricting ourselves to point out the changes due to the GD. First, when GD beads of the first generation are mobile, whereas the core is immobile, Eq. (A7) gets replaced by[18,19]

$$(f-\lambda_k)\Phi_k(1)-\sqrt{f-1}\Phi_k(2)=0 \quad \text{(A23)}$$

and the functions

$$\Phi_k^s(j)=\sin j\psi_k \quad \text{with} \quad j=1,...,g \quad \text{(A24)}$$

in which the ψ_k fulfill

$$\sin(g+1)\psi_k=\sqrt{f-1}\sin g\psi_k, \quad \text{(A25)}$$

solve Eqs. (A6) and (A23) for the eigenvalues λ_k, again given by Eq. (A8).

The number of distinct solutions of Eqs. (A8) and (A25) follows now along the discussion lines after Eq. (A11): The result is that for $(g+1)>\sqrt{f-1}g$ Eqs. (A8) and (A25) have g distinct solutions; otherwise the number of distinct solutions is $(g-1)$. We note[18] that the condition $(g+1)>\sqrt{f-1}g$ is fulfilled only in a few cases, namely, for $f=3$

with $g=1$ and $g=2$ and for $f=4$ with $g=1$. For all other values of the system's parameters we find, based on Eq. (A8), $(g-1)$ distinct eigenvalues, whose eigenmodes are spatially periodic functions of j. In general hence $(g+1) \leqslant \sqrt{f-1}g$ holds, so that one obtains additional eigenmodes. These are of the form[18,19]

$$\Phi(j)=\sinh j\psi \tag{A26}$$

and fulfill Eq. (A5) for Λ given by Eq. (A14). They also fulfill Eq. (A23), whereas Eq. (A6) requires in addition that

$$\sinh(g+1)\psi=\sqrt{f-1}\sinh g\psi \tag{A27}$$

holds. This relation, as discussed above, has a single additional solution ψ if and only if $(g+1)\leqslant\sqrt{f-1}g$. In this way we have in all cases g different eigenvalues. Taking now into account the (f_c-1)-fold degeneracy discussed before, we obtain a total of $(f_c-1)g$ class (ii) normal modes in which next neighbors to the core move.

In general, as discussed before, in class (ii) normal modes even larger groups of noncore beads may stay immobile. We denote by n, with $n<(g-1)$, the last generation in which all beads are immobile. This last generation contains $f_c(f-1)^{n-1}$ immobile beads and we focus on a particular one, to which $(f-1)$ mobile beads are attached. As before, the combination of $(f-1)$ subwedges implies a $(f-2)$-fold degeneracy, so that the total degeneracy is now $f_c(f-1)^{n-1}(f-2)$-fold, with $n\in\{1,...,g-2\}$.

Now for $\Phi_k(j)\equiv 0$ (with $0\leqslant j\leqslant n$) and $\Phi_k(n+1)\neq 0$, Eq. (A5) holds for $n<j<g$, Eq. (A6) stays unchanged, and Eq. (A23) is replaced by[18]

$$(f-\lambda_k)\Phi_k(n+1)-\sqrt{f-1}\Phi_k(n+2)=0. \tag{A28}$$

This leads to the following set of eigenfunctions [see Eqs. (A24) and (A25)]:

$$\Phi_k^s(j)=\sin(j-n)\psi_k, \tag{A29}$$

where the eigenvalues are given by Eq. (A8) and the ψ_k have to be obtained from[18]

$$\sin(g+1-n)\psi_k=\sqrt{f-1}\sin(g-n)\psi_k. \tag{A30}$$

Similar to the cases discussed before, Eq. (A30) has in the interval $0<\psi_k<\pi$ exactly $(g-n)$ distinct solutions if $(g-n+1)>\sqrt{f-1}(g-n)$. Otherwise, i.e., when $(g-n+1)\leqslant\sqrt{f-1}(g-n)$, there are $(g-n-1)$ distinct solutions of the type of Eq. (A29), complemented by one obeying a form akin to Eq. (A26), namely,

$$\Phi(j)=\sinh(j-n)\psi, \tag{A31}$$

whose eigenvalue Λ keeps the form of Eq. (A14), the condition on ψ being now[18]

$$\sinh(g-n+1)\psi=\sqrt{f-1}\sinh(g-n)\psi. \tag{A32}$$

The last equation has a unique nontrivial solution if and only if $(g-n+1)\leqslant\sqrt{f-1}(g-n)$. Thus, taking into account the degeneracies of eigenmodes, we find here a total of $(g-n)f_c(f-2)(f-1)^{n-1}$ eigenvalues.

Finally, in the special situation, $n=(g-1)$, in which only the peripheral beads move, given that $\Phi_k(g-1)=0$, one has[18] from Eq. (A6)

$$(-\lambda_k)\Phi_k(g)+\Phi_k(g)=0. \tag{A33}$$

Equation (A33) has the unique solution $\lambda=1$, which is $f_c(f-1)^{g-2}(f-2)$-fold degenerate.

Paralleling Ref. 18, we obtain now the total number $N_\lambda^{(2)}$ of eigenvalues (relaxation times) for the class (ii) normal modes: Summarizing, in class (ii) one has for each $n\in\{1,...,g-1\}$ exactly $(g-n)$ distinct eigenvalues, which are each $f_c(f-2)(f-1)^{n-1}$-fold degenerate. Including also the case $n=0$, with g distinct eigenvalues, each (f_c-1) times degenerate, leads to

$$N_\lambda^{(2)}=(f_c-1)g+\sum_{n=1}^{g-1}(g-n)f_c(f-2)(f-1)^{n-1}$$

$$=f_c\frac{(f-1)^g-1}{f-2}-g \tag{A34}$$

for $f\geqslant 3$ and to

$$N_\lambda^{(2)}=(f_c-1)g \tag{A35}$$

for $f=2$. We obtain the total number of normal modes, by summing those from class (i), Eq. (A19), and from class (ii), Eqs. (A34) and (A35):

$$N_\lambda=N_\lambda^{(1)}+N_\lambda^{(2)}=N_d, \tag{A36}$$

see Eqs. (4) and (5). Equation (A36) shows that we have indeed found *all* the eigenvalues (relaxation times) of the GD's, with their correct degeneracy.

Finally, the estimation of the minimal eigenvalue in the class (ii) of normal modes proceeds exactly as in Ref. 18. There it was proven that the minimal, nonvanishing eigenvalue corresponds to a spatially exponential normal mode, whose eigenvalue $\Lambda^{(1)}$ obeys[18]

$$\Lambda^{(1)}\simeq\frac{(f-2)^2}{(f-1)^{(g+1)}}. \tag{A37}$$

We note that $\Lambda^{(1)}$ decreases exponentially with g and that it corresponds to a mode in which the largest (main) dendritic branches move as a whole with respect to each other.[18,19]

[1] J. M. J. Fréchet, Science **263**, 1710 (1994).
[2] P. R. Dvornic and D. A. Tomalia, Curr. Opin. Colloid Interface Sci. **1**, 221 (1996).
[3] G. R. Newkome, C. N. Moorefield, and F. Vögtle, *Dendrimers and Dendrons. Concepts, Synthesis, Applications* (Wiley-VCH Verlag, Weinheim, 2001).
[4] R. Yin, Y. Zhu, and D. A. Tomalia, J. Am. Chem. Soc. **120**, 2678 (1998).
[5] V. Percec, C.-H. Ahn, G. Ungar, D. J. P. Yeardly, M. Möller, and S. S. Sheiko, Nature (London) **391**, 161 (1998).
[6] S. Jahromi, B. Coussens, N. Meijerink, and A. W. M. Braam, J. Am. Chem. Soc. **120**, 9753 (1998).
[7] S. Jahromi, J. H. M. Palmen, and P. A. M. Steeman, Macromolecules **33**, 577 (2000).
[8] S. Jahromi, V. Litvinov, and B. Coussens, Macromolecules **34**, 1013 (2001).
[9] J. W. Kriesel and T. D. Tilley, Chem. Mater. **11**, 1190 (1999).
[10] W.-D. Jang, D.-L. Jiang, and T. Aida, J. Am. Chem. Soc. **122**, 3232 (2000).
[11] F. Gröhn, G. Kim, B. J. Bauer, and E. J. Amis, Macromolecules **34**, 2179 (2001).
[12] I. Gitsov and C. Zhu, Macromolecules **35**, 8418 (2002).
[13] P. R. Dvornic, J. Li, A. M. de Leuze-Jallouli, S. D. Reeves, and M. J. Owen, Macromolecules **35**, 9323 (2002).
[14] A. A. Gurtovenko and A. Blumen, J. Chem. Phys. **115**, 4924 (2001).

[15] A. A. Gurtovenko and A. Blumen, Macromolecules **35**, 3288 (2002).
[16] P. E. Rouse, J. Chem. Phys. **21**, 1272 (1953).
[17] M. Doi and S. R. Edwards, *The Theory of Polymer Dynamics* (Clarendon, Oxford, 1986).
[18] A. A. Gurtovenko, Yu. Ya. Gotlib, and A. Blumen, Macromolecules **35**, 7481 (2002).
[19] Yu. Ya. Gotlib and D. A. Markelov, Polym. Sci. U.S.S.R. **A44**, 1341 (2002) (translated from Vysokomol. Soedin., Russia).
[20] J.-U. Sommer and A. Blumen, J. Phys. A **28**, 6669 (1995).
[21] H. Schiessel, Phys. Rev. E **57**, 5775 (1998).
[22] H. Schiessel, C. Friedrich, and A. Blumen, in *Applications of Fractional Calculus in Physics*, edited by R. Hilfer (World Scientific, Singapore, 2000), p. 331.
[23] C. Satmarel, A. A. Gurtovenko, and A. Blumen, Macromolecules **36**, 486 (2003).
[24] J. D. Ferry, *Viscoelastic Properties of Polymers*, 3rd edition (Wiley, New York, 1980).
[25] H. Yamakawa, *Modern Theory of Polymer Solutions* (Harper and Row, New York, 1971).
[26] W. W. Graessley, Macromolecules **13**, 372 (1980).
[27] P. G. de Gennes and H. Hervet, J. Phys. (Paris) **44**, L351 (1983).
[28] A. Kloczkowski, J. E. Mark, and H. L. Frisch, Macromolecules **23**, 3481 (1990).
[29] P. Biswas and B. J. Cherayil, J. Chem. Phys. **100**, 3201 (1994).
[30] D. Boris and M. Rubinstein, Macromolecules **29**, 7251 (1996).
[31] C. Cai and Z. Y. Chen, Macromolecules **30**, 5104 (1997).
[32] R. La Ferla, J. Chem. Phys. **106**, 688 (1997).
[33] Z. Y. Chen and C. Cai, Macromolecules **32**, 5423 (1999).
[34] F. Ganazzoli and R. La Ferla, J. Chem. Phys. **113**, 9288 (2000).
[35] F. Ganazzoli, R. La Ferla, and G. Terragni, Macromolecules **33**, 6611 (2000).
[36] F. Ganazzoli, R. La Ferla, and G. Raffaini, Macromolecules **34**, 4222 (2001).
[37] P. Biswas, R. Kant, and A. Blumen, Macromol. Theory Simul. **9**, 56 (2000).
[38] P. Biswas, R. Kant, and A. Blumen, J. Chem. Phys. **114**, 2430 (2001).
[39] R. L. Lescanec and M. Muthukumar, Macromolecules **23**, 2280 (1990).
[40] M. L. Mansfield and L. I. Klushin, Macromolecules **26**, 4262 (1993).
[41] M. Murat and G. S. Grest, Macromolecules **29**, 1278 (1996).
[42] Z. Y. Chen and S.-M. Cui, Macromolecules **29**, 7943 (1996).
[43] A. V. Lyulin, G. R. Davies, and D. B. Adolf, Macromolecules **33**, 3294 (2000).
[44] J. S. Ham, J. Chem. Phys. **26**, 625 (1957).
[45] Yu. Ya. Gotlib and K. M. Salikhov, Akust. Zh. **9**, 301 (1963).
[46] A. J. Chompff and J. A. Duiser, J. Chem. Phys. **45**, 1505 (1966).
[47] A. A. Gurtovenko and Yu. Ya. Gotlib, Macromolecules **31**, 5756 (1998).
[48] A. A. Gurtovenko and Yu. Ya. Gotlib, Macromolecules **33**, 6578 (2000).
[49] C. Kittel, *Introduction to Solid State Physics*, 6th edition (Wiley, New York, 1986).
[50] N. W. Ashcroft and N. D. Mermin, *Solid State Physics* (Sanders College, Philadelphia, 1981).
[51] J. M. Ziman, *Principles of the Theory of Solids*, 2nd edition (Cambridge University Press, Cambridge, 1972).
[52] Yu. Ya. Gotlib and A. A. Gurtovenko, Macromol. Theory Simul. **9**, 407 (2000).
[53] A. A. Gurtovenko and Yu. Ya. Gotlib, Macromol. Theory Simul. **9**, 416 (2000).
[54] S. Uppuluri, S. E. Keinath, D. A. Tomalia, and P. R. Dvornic, Macromolecules **31**, 4498 (1998).